The structure of the RNA-dependent RNA polymerase from bovine viral diarrhea virus establishes the role of GTP in *de novo* initiation

Kyung H. Choi*, James M. Groarke†‡, Dorothy C. Young†, Richard J. Kuhn*, Janet L. Smith*, Daniel C. Pevear†, and Michael G. Rossmann*§

*Department of Biological Sciences, Purdue University, 915 West State Street, West Lafayette, IN 47907; and †Department of Biology, ViroPharma, Incorporated, 405 Eagleview Boulevard, Exton, PA 19341

Contributed by Michael G. Rossmann, January 31, 2004

The bovine viral diarrhea virus (BVDV) RNA-dependent RNA polymerase can initiate RNA replication by a *de novo* mechanism without a primer. The structure of BVDV polymerase, determined to 2.9-Å resolution, contains a unique N-terminal domain, in addition to the fingers, palm, and thumb domains common to other polymerases. The structure of BVDV polymerase complexed with GTP, which is required for *de novo* (primer-independent) initiation, shows that GTP binds adjacent to the initiation NTP, suggesting that the GTP mimics a vestigial RNA product. Comparison of five monomers in two different crystal forms showed conformational changes in the fingertip region and in the thumb domain that may help to translocate the RNA template and product strands during elongation. The putative binding sites of previously reported BVDV inhibitors are also discussed.

The function of a polymerase is to synthesize the complementary RNA or DNA molecule from a template strand. Thus, the polymerase requires binding sites for the template, nucleoside triphosphates (NTPs or dNTPs), and the nascent polynucleotide product. Also required are mechanisms to catalyze the addition of NTP or dNTP to the nascent chain, to recognize the next complementary NTP molecule, and to move the template and product by one nucleotide in readiness for the next elongation event. Finally, the polymerase, in conjunction with other viral and cellular enzymes, such as a helicase in a replication complex, requires a mechanism for initiating and terminating synthesis of the new product polynucleotide.

RNA replication in positive-sense single-stranded (ss)RNA viruses is initiated at or near the 3′ end of the template using either primer-dependent or primer-independent (*de novo*) mechanisms. Poliovirus, for example, utilizes a genome-linked protein as a primer for initiation of RNA synthesis (1). In *Flaviviridae*, on the other hand, *de novo* initiation is the likely mechanism used during virus replication in infected cells (2). In *de novo* initiation, the second NTP is added (with the release of its pyrophosphate moiety) directly to the 3′-OH of the first initiation NTP without the need of a primer. This nucleotidyl transfer reaction is then repeated with subsequent NTPs to generate the complementary RNA product. *De novo* initiation by *Flaviviridae* RNA polymerases requires (*i*) a template RNA with a virus-specific initiation nucleotide at the 3′ end, (*ii*) a complementary initiation NTP, and (*iii*) GTP (3–6). Because base pairing between the template RNA and individual NTPs may not be sufficient to allow the formation of a stable initiation complex, it is likely that *de novo* initiation requires specific molecular interactions among the template RNA, NTPs, the RNA polymerase, and possibly other viral and host proteins. Although not all RNA-dependent RNA polymerases (RdRps) require GTP for initiating RNA synthesis, other ligands or structural components can act similarly as GTP and help to position the 3′-OH group of the priming nucleotide ready for nucleophilic attack.

The *Flaviviridae* family consists of three genera: the flaviviruses (including dengue, West Nile, and yellow fever viruses), hepacivirus (hepatitis C virus, HCV), and the pestiviruses [including bovine viral diarrhea virus (BVDV)]. Pestiviruses are animal pathogens of major importance, particularly to the livestock industry. They show greater similarity in genome structure and translation strategy to hepaciviruses than to flaviviruses (7). Because hepaciviruses, which infect 3% of the world population, are difficult to grow in cell culture, pestiviruses have been used as a model system for investigating hepaciviruses. BVDV, the best-studied pestivirus, has a genome that consists of an ≈12.6-kb positive-sense ssRNA (8). The BVDV genome is translated into a single polyprotein represented by NH_2-N^{pro}-C-E^{rns}-E1-E2-P7-NS2-NS3-NS4A-NS4B-NS5A-NS5B-COOH, where N^{pro} is the N-terminal autoprotease, C is the capsid protein, E^{rns} is an envelope glycoprotein with RNase activity, E1 and E2 are external envelope glycoproteins, and P7 is a 7-kDa protein of unknown function. The polyprotein is processed into at least four structural (C, E^{rns}, E1, and E2) and six nonstructural (NS2, NS3, NS4A, NS4B, NS5A, and NS5B) proteins required for viral assembly and replication (7, 8). Among the NS proteins, the functions of NS3, NS4A, and NS5B have been most extensively characterized. NS3 contains a viral serine protease domain (sometimes requiring NS4A as a cofactor) and a helicase/NTPase domain. NS5B is an RdRp and is responsible for genome replication as a part of a larger, membrane associated, replicase complex (7).

The crystal structures of RdRps from various families of single- or double-stranded RNA viruses have been determined [HCV (9–13), calicivirus (14), poliovirus (15), ϕ6 (16), and reovirus (17)]. In addition, the structures of several DNA polymerases have been determined, including the DNA-dependent DNA polymerase Klenow fragment from *Escherichia coli* (18) and HIV type 1 reverse transcriptase (19–22). Although there is low sequence identity between polymerases (23), they all have roughly the shape of a right hand with fingers, palm, and thumb domains. During elongation, the template and product move along a channel, formed by the thumb and fingers, toward the palm domain, which contains the catalytic residues. The thumb domain might serve to ratchet the template and product over the surface of the hand with its exposed catalytic site (16).

Here, we present the crystal structure of a truncated form of the BVDV polymerase determined to 2.9-Å resolution by x-ray crystallography. The polymerase structure possesses a unique N-terminal domain, in addition to the conserved "core," common to other polymerases. Like the HCV and ϕ6 polymerases, the BVDV polymerase utilizes a motif in the thumb domain to completely

Abbreviations: BVDV, bovine viral diarrhea virus; HCV, hepatitis C virus; NTP, nucleotide triphosphate; RdRp, RNA-dependent RNA polymerase; SeMet, selenomethionine; ssRNA, single-stranded RNA.

Data deposition: The atomic coordinates have been deposited in the Protein Data Bank, www.pdb.org [PDB ID codes 1S48 (form 1 crystals), 1S4F (form 2 crystals), and 1S49 (form 1 complexed with GTP)].

‡Present address: Novartis Pharmaceuticals, One Health Plaza, Building 435, East Hanover, NJ 07936.

§To whom correspondence should be addressed. E-mail: mgr@indiana.bio.purdue.edu.

BIOPHYSICS

Table 1. BVDV data collection and refinement statistics

	MAD (SeMet)			SAD (SeMet)	GTP	VP32947	Native
Data processing*							
Constructs	71–679			71–679	71–679	71–679	79–678
Wavelength, Å	0.9797	0.9795	0.9568	0.9795	0.928	0.928	1.0
Space group	$P6_222$ (form 1)			$P6_222$ (form 1)	$P6_222$ (form 1)	$P6_222$ (form 1)	$P6_222$ (form 2)
Cell dimensions, Å	$a = b = 206.0$, $c = 99.4$			$a = b = 205.7$, $c = 99.6$	$a = b = 206.1$, $c = 99.6$	$a = b = 204.9$, $c = 102.1$	$a = b = 412.3$, $c = 95.6$
Resolution, Å	30–3.4	30–3.4	30–3.4	40–3.0	30–2.3	30–3.4	30–2.9
Reflections							
Observed	371,529	376,271	357,766	1,028,434	561,175	191,942	1,104,340
Unique	32,443¶	32,451¶	32,398¶	47,219¶	55,339	17,850	105,317
Completeness, %	98.5 (99.5)	98.5 (99.5)	98.3 (99.6)	99.9 (99.9)	99.7 (100)	99.7 (100)	99.7 (100)
Mean I/σ	20 (4.3)	20 (5.6)	20 (2.9)	25 (3.3)	23 (3.9)	24 (5.1)	18 (3.6)
R_{merge}, %†	0.16 (0.67)	0.17 (0.56)	0.16 (0.71)	0.135 (0.70)	0.09 (0.46)	0.11 (0.50)	0.14 (0.82)
Refinement							
R_{cryst}, %‡				22.4			25.5
R_{free}, %§				27.4			30.4
No. of atoms				4732			18718
Average *B*-factor				48.4			50.5
rms deviation from ideal							
Bond length, Å				0.0084			0.0085
Bond angle, °				1.64			1.64

MAD, multiple-wavelength anomalous dispersion; SAD, single-wavelength anomalous dispersion.
*The numbers in parentheses refer to the highest-resolution shell.
†$R_{merge} = \Sigma_{hkl}|I(hkl)-\langle I(hkl)\rangle|/\Sigma_{hkl}\langle I(hkl)\rangle$.
‡$R_{cryst} = \Sigma_{hkl}|F_o(hkl)-F_c(hkl)|/|F_o(hkl)$.
§$R_{free} = R_{cryst}$, calculated for 10% randomly selected reflections that are not included in the refinement.
¶Friedel opposites are each counted for noncentric reflections.

encircle the active site cavity. We have now determined the structure of BVDV polymerase complexed with GTP and identified the GTP-specific binding site required for *de novo* initiation. Comparison of four independent monomers in the crystallographic asymmetric unit of another BVDV RdRp construct shows conformational flexibility that may be important for the translocation of the template and product during RNA elongation.

Methods

Expression and Purification of BVDV Polymerase. Based on limited proteolysis and multiple sequence alignment, eighty-four truncation constructs of BVDV polymerase were designed representing combinations of variable N and C termini with N- or C-terminal hexahistidine affinity tags. DNAs encoding the variant polymerases were cloned and expressed in a high-throughput system (unpublished work). The hexahistidine affinity-tagged proteins were purified on Talon resin (Clontech) and eluted with 30–50 mM imidazole in extraction/wash buffer (Clontech). BVDV polymerase was further purified by cation exchange chromatography using Poros-HS (PerSeptive Biosystems, Framingham, MA).

Crystallization. Purified BVDV polymerase was buffer-exchanged into 20 mM Tris·Cl, pH 7.5, containing 0.3 M NaCl, 5% glycerol, and 2 mM DTT, and concentrated to ≈9 mg/ml. Initial crystallization trials were conducted by using vapor diffusion with sitting drops in 96-well crystallization plates. Crystals of two different BVDV polymerases (Table 1) suitable for x-ray analysis (0.1 × 0.2 × 0.05 mm) grew in 1–4 weeks in 1.9 M ammonium sulfate and 3–5% isopropanol.

Selenomethionine Protein Preparation. Selenomethionine (SeMet) protein was produced and purified for use in a MAD experiment. The Met auxotroph *E. coli* B834 (DE3) was transformed with a plasmid encoding BVDV polymerase and plasmid RIL encoding rare codon tRNAs. Cells were grown in M9 minimal media (24, 25) (supplemented with 19 amino acids, SeMet, and vitamins) and induced with 1.5 mM isopropyl β-D-thiogalactoside. Purification of SeMet protein was similar to that of native protein, except that 10 mM DTT was added to all buffers after the Talon column to prevent oxidation of incorporated SeMet. Mass spectrometry of both the native and SeMet proteins verified the presence of 12 SeMet residues, consistent with the 12 Met residues in the protein.

Structure Determination. Crystals (form 1) of the BVDV construct (residues 71–679 with a C-terminal His tag) were transferred to a cryoprotectant solution in a step-wise manner and frozen in liquid nitrogen. A three-wavelength anomalous dispersion data set was collected at the Se fluorescence peak, inflection point, and a remote wavelength. Additionally, a SAD data set was collected at the Se peak. Both data sets were collected at Advanced Photon Source beamline 14ID-B. Data were indexed with DENZO (26) and scaled and merged with SCALEPACK (26). Initial indexing and merging indicated that the crystals belong to the space group $P6_222$ or $P6_422$, with $a = b = 206.0$, $c = 99.4$ Å.

Positions of all 12 Se sites were located by using the program SOLVE (27) and the MAD data set. Density modification of the initial MAD-phased electron density produced an interpretable map. Although both the 3.4-Å-resolution MAD and the 3.0-Å-resolution SAD phases produced interpretable maps, the SAD map appeared more interpretable and was used for initial model building with the program O (28). The model was refined by using simulated annealing as implemented in CNS (29) (Table 1).

A second BVDV polymerase construct (residues 79–678 with an N-terminal hexahistidine tag) produced crystals of form 2 that also belonged to space group $P6_222$, but with cell dimensions of $a = b = 412.3$, $c = 95.6$ Å. The structure was determined by the molecular replacement method (30, 31) and refined as described above (Table 1).

Polymerase Complexes with GTP. The BVDV polymerase incorporating SeMet (residues 71–679 with a C-terminal hexahistidine tag) was cocrystallized with 10 mM GTP. Data were collected at Cornell High Energy Synchrotron Source beamline F1. The crystals were isomorphous with the form 1 crystals. A difference map contoured

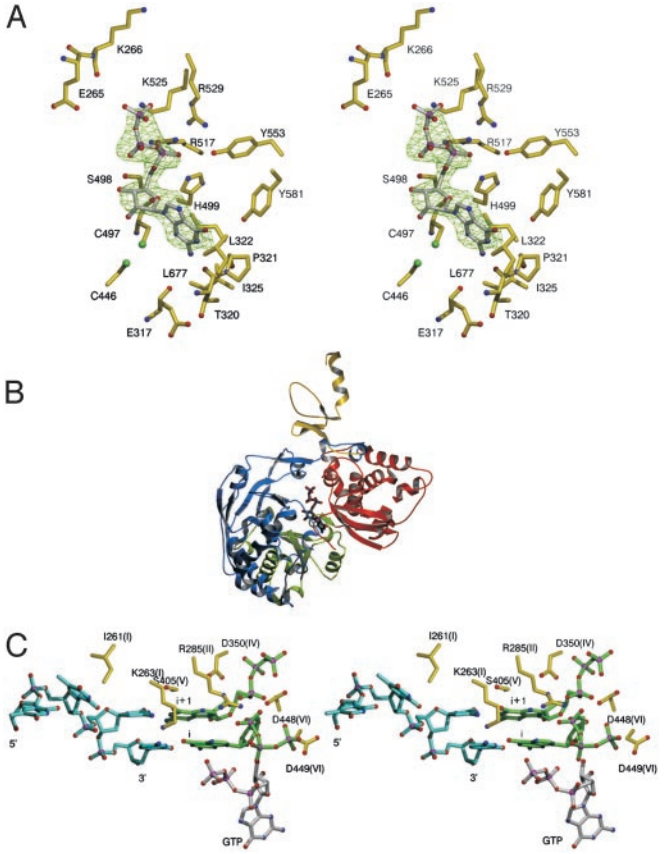

Fig. 1. The BVDV active site. (*A*) Stereoview of the GTP-binding site. The difference electron density map is displayed as a green wire cage. The residues involved in the GTP-binding site are depicted as ball-and-stick models. (*B*) The BVDV structure, in the same orientation, showing the bound GTP molecule in thick black. (*C*) Stereoview of the BVDV (yellow) polymerase active site. The position of the template and NTP sites were derived by superposition of the ϕ6 polymerase structure. The motif number (I,II,. . .) is given in parentheses with each active site residue labeled. The template is shown in cyan; the NTPs at the *i* (priming) and *i* + 1 (catalytic) sites are shown in green. The GTP in the BVDV polymerase structure is shown in gray.

at 2.5σ showed clear density into which a GTP molecule was easily fitted (Fig. 1).

Results

Crystallization and Structure Determination of BVDV Polymerase. BVDV polymerase was expressed in *E. coli* and purified as a soluble protein. A crystallizable protein was obtained by truncation of the first 70 and the last 40 amino acids, which included the highly hydrophobic C-terminal residues where the putative membrane-anchoring region is located. BVDV polymerase crystallized with one monomer in the asymmetric unit forming a dimer across a crystallographic two-fold axis. The final model of BVDV polymerase at 2.9-Å resolution contains 580 of the 601 residues of the truncated molecule. The first 20 N-terminal residues were not observed in the electron density map (Table 1).

The Fingers, Palm, and Thumb Domains. The BVDV polymerase core (residues 139–679) has a roughly spherical shape with dimensions of ≈74 × 60 × 58 Å around a central cavity. In addition, there is an N-terminal region (residues 71–138) of which residues 71–91 are disordered (see Fig. 2 for secondary structure nomenclature).

The fingers domain (residues 139–313 and 351–410) consists of 12 α-helices and 11 β-strands. In BVDV RdRp, as in other viral RdRps, the N terminus of the fingers domain, together with a long

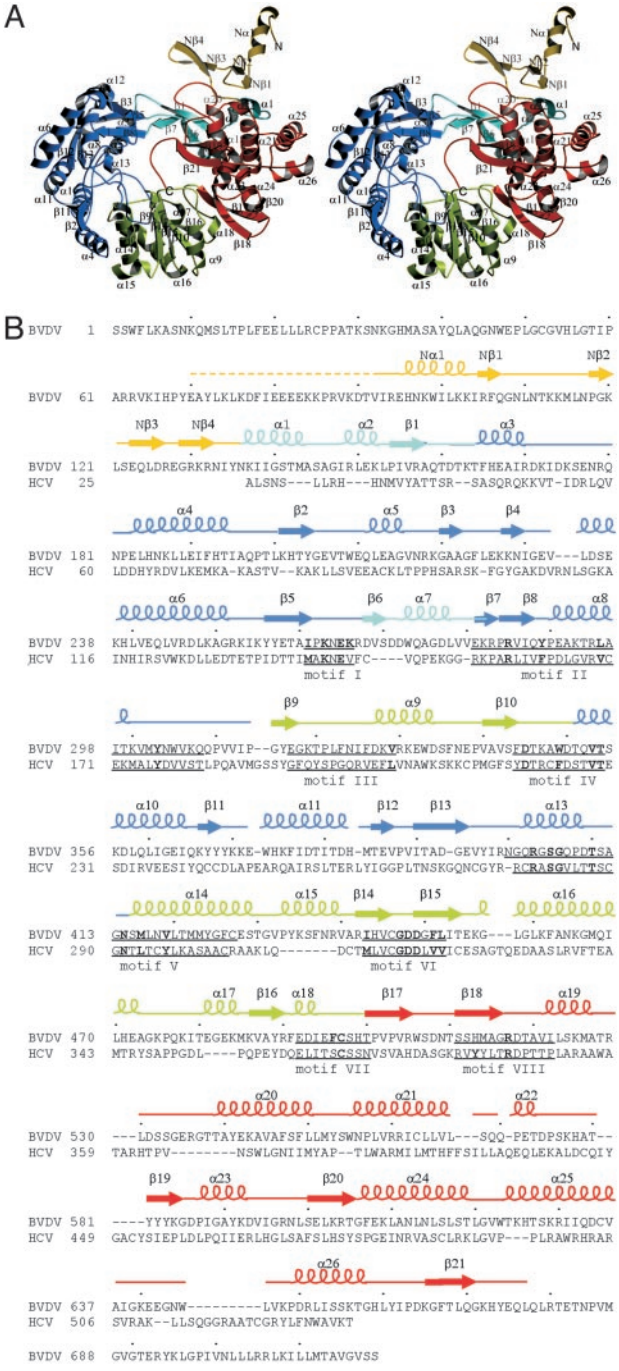

Fig. 2. The BVDV polymerase structure. (*A*) Stereoview of the structure of BVDV polymerase. The N-terminal, fingers, palm, and thumb domains are colored yellow, blue, green, and red, respectively. The fingertip region is shown in cyan. Secondary structural elements, as well as the N and C termini, are labeled. (*B*) BVDV and HCV polymerase amino acid alignment, based on a least-squares minimization of equivalent C_α atoms. The secondary structure assignment is based on the BVDV polymerase structure. α-Helices and β-strands are shown as coils and arrows, respectively. Disordered regions are shown as dotted lines. The regions that were not included in the polymerase construct are left blank. The eight polymerase motifs are underlined, and completely conserved residues are in bold. The domains are color-coded as in *A*.

insert in the fingers domain (residues 260–288), form a fingertip region that associates with the thumb domain. The conformation of the polypeptide chain in the fingertip region differs among RdRps (Fig. 3). For example, whereas BVDV polymerase has a three-

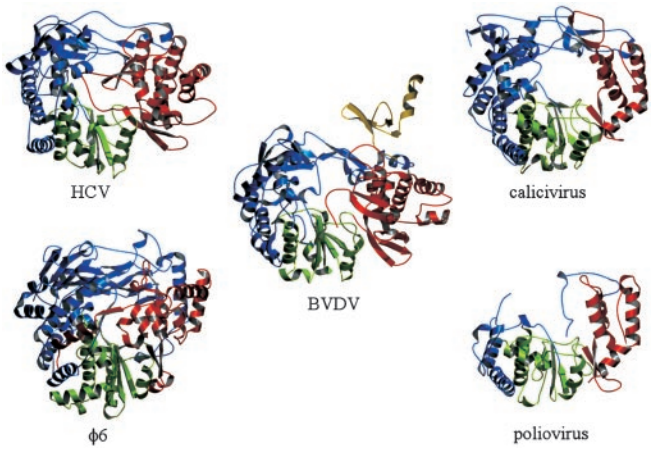

Fig. 3. Comparison of RdRp structures. BVDV, HCV, ϕ6, poliovirus, and calicivirus RdRps are shown in the conventional orientation as if looking into a right hand. The fingers domain of the poliovirus polymerase structure is mostly disordered. The domains are colored according to the conventions of Fig. 2*A*.

stranded fingertip region, HCV (9–13) and calicivirus polymerases (14) have a four-stranded and ϕ6 polymerase (16) has a six-stranded fingertip region. The fingers and thumb domains are associated through the fingertip region, thus the conformational change induced by template binding into the central channel may be limited (9, 10). The remainder of the fingers domain is comprised of a β-strand-rich region (β-fingers) and an α-helix-rich region (α-fingers) close to the palm domain. Although there is little sequence identity, the topology of the fingers domain, excluding the fingertips, is similar to that of other viral polymerases, making possible the structural alignment of the BVDV, HCV, calicivirus, and ϕ6 polymerase fingers domains. As expected, BVDV polymerase has greater structural similarity to HCV polymerase, indicating a closer evolutionary link between theses two viruses than with the other viruses.

The palm domain is the catalytic domain and shows the greatest structural conservation among all known polymerases. The palm domain of BVDV polymerase (residues 314–350, 411–500) consists of a four-stranded β-sheet flanked by two α-helices on one side and an additional α-helix on the other side of the β-sheet, nested between the palm and thumb domains. Compared to HCV polymerase, BVDV polymerase has a small α-helix (residues 433–439) inserted immediately before the first β-strand (β14) of the β-sheet. A comparative analysis of RNA polymerase sequences in positive-strand RNA viruses has identified eight conserved sequence motifs, I-VIII (23, 32). Five of these motifs are in the palm domain, including the Gly-Asp-Asp (GDD) motif VI, which is essential for catalytic activity (33).

The thumb domain, consisting of the C-terminal region of the polypeptide chain, is the most diverse feature among the known polymerase structures. The thumb domain of BVDV polymerase (residues 501–679) contains eight α-helices and five β-strands and is larger than the thumb domain of other viral RdRps (Fig. 3). Although there is some structural similarity between the HCV and BVDV thumb domains, the overall topology is rather different. The BVDV polymerase thumb domain possesses a structural element ("the β-thumb region") in which two β-strands (β19 and β21) and their connecting loops form a layer that occludes the active site cavity. The β-thumb region interacts with the fingers and palm domains through a long C-terminal loop (residues 670–679), tucked between the palm and thumb domains. Together with a loop between α20 and α21 in the thumb domain, the β-thumb reduces the volume of the template channel (Fig. 3).

A similar protrusion into the active site, formed by a β-hairpin, is present in the HCV polymerase structure, although the protrusion originates from a different part of the thumb domain (Fig. 3). An HCV polymerase mutant, in which the β-hairpin (residues 446–463) was replaced with a shorter turn, was able to use template–primer complexes that the wild-type enzyme was unable to use (34). Thus, the β-thumb in BVDV polymerase may have a similar function as the β-hairpin in HCV polymerase in allowing only ssRNA access to the active site during initiation. Similarly, the double-stranded RNA phage ϕ6 polymerase, which is capable of directing *de novo* initiation from ssRNA, has its C-terminal region protruding into the active site. In contrast, poliovirus and calicivirus polymerases, which initiate using a template and primer, lack such β-hairpin loops (14). These enzymes have a wider channel that can accommodate a template–primer complex for initiation. Thus, it seems that discrimination between primer-dependent and -independent initiation is accomplished by restricting access to the template-binding site.

N-Terminal Domain. The BVDV RdRp is ≈130 residues longer at its N terminus than HCV RdRp (33). The function of this N-terminal domain is not known, although up to 90 residues can be truncated from BVDV polymerase without loss of polymerase activity *in vitro* (33). It has been suggested that the N-terminal region in other polymerases is required for binding proteins in the replication complex (35).

The ordered part of the N-terminal region (residues 92–138) folds into a separate domain. The N-terminal domain is situated over the thumb domain, interacting with the fingertip region and thumb domain through a β-hairpin motif (Nβ3-loop-Nβ4) (Fig. 2*A*). The β-hairpin motif points toward the template channel and partially occludes the channel entrance, possibly explaining why some N-terminal truncated proteins have greater polymerase activity than wild type (33).

The entrance to the template-binding channel created by the β-hairpin motif of the N-terminal domain is highly positively charged. An equivalent positively charged surface at the entrance to the channel was found in ϕ6 polymerase, where it was proposed to act as a "plough" that unwinds the double-stranded RNA, thus aiding the function of a helicase (16). Similarly in BVDV polymerase, this positively charged surface may be used to open up RNA secondary structural hairpins before the ssRNA template entering the active center.

Initiation Complex of RNA Polymerase with GTP. A high concentration of GTP (but not any other nucleotide) is required for *de novo* initiation of RNA synthesis in BVDV (3, 36), as well as in other members of the *Flaviviridae* family (4–6), regardless of the nucleotide at the 3′ end of the RNA template. The structure of BVDV polymerase, complexed with GTP, shows that GTP binds 6 Å from the catalytic GDD-containing motif, inside the template-binding channel. The GTP molecule interacts extensively with the polymerase through a hydrogen-bonding network, electrostatic interactions, and hydrophobic interactions with residues from all three polymerase domains (Fig. 1*A*). The orientation of GTP that was fitted into the difference electron density map is supported by the basic environment of the phosphate groups (His-499, Arg-517, Lys-525, Arg-529), by the polar environment of the ribose OH groups (Cys-446, Cys-497, Ser-498), by the hydrophobic environment around the guanine base (Pro-321, Leu-322, Leu-677), and by hydrogen bonds of guanine N1 and N2 with the main-chain carbonyl of Thr-320, as well as O6 with the OH group of Tyr-581. With the exception of the hydrogen bond to N1, these bonds provide specificity for guanine, as opposed to adenine. In contrast, the NTP-binding sites (see below) are created only in the presence of bound template. The GTP-binding site in BVDV polymerase is within ≈4 Å of the nearest NTP site, compared to their positions in HCV or φ6 polymerase complex (Fig. 1*C*). Thus, the polymerase–GTP complex presented here is probably the GTP–polymerase complex required for initiation of RNA synthesis.

Most of the residues involved in the GTP-binding site are in the RdRp motifs III, VII, and VIII. Some of the residues in motifs VII and VIII (including Cys-497, Ser-498, and Arg-517) have been mutated individually to alanine and tested for their ability to direct RNA synthesis via primer-dependent (elongative) and -independent (*de novo*) mechanisms (33). Primer-dependent RNA elongation was reduced by only 2- to 10-fold, whereas *de novo* synthesis was almost completely abolished. This discrimination between the two possible modes of initiation was observed only when the three residues mentioned above were mutated, and not when similar mutations were made in other conserved motifs. Similar discrimination has been demonstrated by mutating Arg-386 in HCV polymerase, equivalent to Arg-517 in BVDV polymerase (37), confirming that the GTP-binding site described here is essential for *de novo* initiation of RNA synthesis in *Flaviviridae* polymerases.

Discussion

Model for RNA Template Binding. Of the extensive structural data, the ϕ6 and HCV RdRps proved to be the most useful because of the high degree of structural homology to BVDV RdRp. In the ϕ6 polymerase–template–NTP complex, there are two NTP sites, *i* [the priming site (16)] and $i + 1$ (the catalytic site) surrounding the GDD residues essential for RNA synthesis. Both NTPs are base-paired with template bases. The NTP *i* site, closer to the 3′ end of the template, corresponds to the last base added to the growing RNA oligonucleotide, whereas the NTP $i + 1$ site would correspond to the next incoming nucleotide. The 3′-OH group of the NTP at the *i* site is oriented correctly for a nucleophilic in-line attack on the α-phosphate of the incoming NTP at the $i + 1$ site. Thus, the ϕ6 polymerase structure shows the organization of the template and its base-paired product as expected for elongation.

A model for RNA template binding in BVDV polymerase was based on the ϕ6 polymerase template and polymerase template–NTP complexes (PDB ID codes 1HHT and 1HI0), as well as the HCV polymerase–template complex (ID code 1NB7). Superposition of the conserved palm domains of ϕ6 and HCV polymerase onto the BVDV polymerase palm domain brings the fingers domains of all three polymerases into good agreement. The overall superposition of fingers and palm domains results in rms deviations of 3.2 Å for 234 topologically equivalent C_α atoms of ϕ6 polymerase and 2.3 Å for 247 C_α atoms of HCV polymerase. The position and orientation of the ϕ6 and HCV RNA template strand when placed into the BVDV polymerase structure are similar. In both superpositions, the ssRNA template is easily accommodated by the BVDV polymerase active site with few steric clashes. The entrance to the template channel is restricted by the β-hairpin from the N-terminal domain but is large enough to allow the 3′ end of the template strand to enter the active site. The phosphate backbone of the template interacts with residues mainly from the fingers domain. The RdRp motif II is in contact with the phosphate backbone and bases, indicating the role of this motif in template binding. In addition, motif I is close to the NTP $i + 1$ binding site, indicating its function for binding the incoming NTP.

When the ϕ6 polymerase–NTP template structure was superimposed onto the BVDV–GTP complex structure, the ribose triphosphate moiety of GTP was found to be positioned as might be expected for an $i-1$ site of a synthesized RNA strand (Fig. 1*B*). The 3′-hydroxyl of the GTP ribose is positioned near the α- and β-phosphates of the NTP at the *i* site. Thus, the GTP may provide a vestigial synthesized RNA molecule that can initiate elongation of the complementary strand. A similar role for orienting the priming NTP has been proposed for the "priming loop" of reovirus RdRp (17). Various dinucleotides can replace GTP for *de novo* initiation in pestiviruses and HCV polymerases (36). These dinucleotides have a guanosine at their 3′ end that acts as an initiation nucleotide when complexed with template and polymerase, leaving the 5′ end of the dinucleotide to protrude beyond the 3′ end of the template. The ability of these dinucleotides to initiate RNA synthesis could be explained by recognizing that the 3′ end of the dinucleotide would be positioned at the *i* site and the 5′end of the dinucleotide would be at the GTP-binding site, the latter thus providing the initiation complex normally associated with the bound GTP.

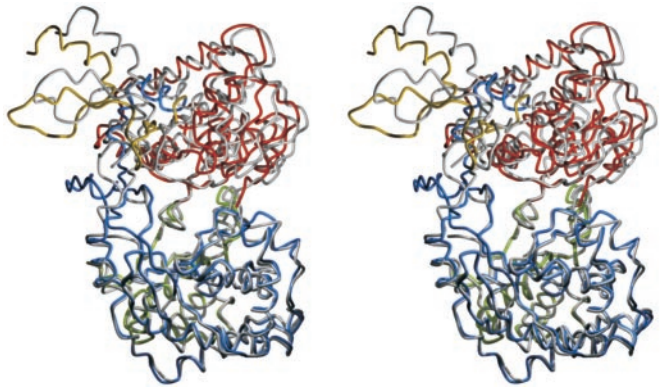

Fig. 4. Conformational differences between BVDV monomers in different crystal forms. The domains of the monomer in crystal form 1 are shown with the same color code as used in Fig. 2*A*. Monomer D from crystal form 2 is shown in gray.

Conformational Changes in BVDV Polymerase. The structure described above (residues 71–679 with a C-terminal hexahistidine tag) has one molecule per asymmetric unit of form 1 crystals. However, a construct consisting of residues 79–678 and an N-terminal hexahistidine tag had four molecules per crystallographic asymmetric unit of form 2 crystals. These four monomers are arranged as two noncrystallographic dimers, AB and CD, each of which is similar to the crystallographic dimer in the smaller (form 1) unit cell. Because each of the four monomers in the asymmetric unit is in a slightly different environment, structural differences between monomers might provide insight into inherent structural flexibility and conformational changes in BVDV polymerase.

Superposition of the structure determined in the smaller (form 1) unit cell onto each of the four monomers in the form 2 crystal gives a rms deviation of <1.0 Å for monomers A, B, and C, but 8 Å for monomer D (calculated over all equivalent C_α atoms). When only the fingers and palm domains were superimposed, monomer D differed from monomers A, B, C, and the monomer in the form 1 crystal in that the thumb domain was rotated by $\approx$8°, the N-terminal domain was rotated by $\approx$13°, and residues 268–276 in the fingertip region have a changed conformation (Fig. 4). In addition, Ser-532-Glu-537 and Lys-672-Glu-675 in the β-thumb deviate in their conformation among the five copies of the molecule. Furthermore, residues 277–282 of the fingertip region, as well as residues 530–532 in the thumb domain of monomer D, are disordered. The fingertip region contains RdRp motif II, which is involved in NTP binding, and the β-thumb occludes the active site.

Movement of the fingertip region associated with the binding of each subsequent NTP to be incorporated into the growing RNA product, in conjunction with a rotation of the thumb domain forming part of the template channel, may help translocate the template and product for each elongation step.

Mutations Conferring Resistance to BVDV Polymerase Inhibitors. Two inhibitors of BVDV RNA replication that target the polymerase have been reported (38, 39). Baginski *et al.* (38) describe a small 329-Da noncompetitive inhibitor {3-[((2-dipropylamino)ethyl)-thio]-5H-1,2,4-triazino[5,6-b]indol}, VP32947, which blocks viral RNA synthesis *in vitro* and *in vivo*. The potency of the compound against BVDV replication in cell culture ($EC_{50} = \approx$20 nM) was significantly greater than its activity against purified polymerase in a biochemical assay ($IC_{50} = \approx$700 nM) (38). Several drug-resistant

BIOPHYSICS

variants of BVDV were selected and shown to have Ser substituted for Phe at position 224 in the viral polymerase. When this single amino acid change was introduced into an infectious clone of wild-type virus, replication of the resulting variant virus was resistant to VP32947. Phe-224 is ≈20 Å away from the active site, located in a fingers domain surface loop that points toward the fingertip region. The location of Phe-224 is consistent with the noncompetitive nature of the inhibitor, suggesting that the drug-binding site does not overlap with the substrate-binding site. Phe-224, near the putative binding site of VP32947, makes hydrophobic interactions with Ile-390, Ala-392, and Leu-225. Thus, this compound could inhibit the normal flexibility of the fingers (40), which may be required for translocation of the template and product (see above).

Phe-224 is located in the dimer interface created by a crystallographic two-fold axis, which produces contacts between the N-terminal domain of one monomer and the fingers domain of another in the form 1 crystals. The same interface occurs in the AB and CD noncrystallographic dimers in crystal form 2. Thus, the binding site for VP32947 may be in the dimer interface of the crystalline polymerase, making it difficult for the compound to bind to either of the two crystal forms described here. This is consistent with the absence of bound inhibitor in crystals into which 1 mM VP32947 was diffused for >2 h (Table 1). Dynamic light-scattering and gel filtration experiments showed that BVDV polymerase is a monomer in solution (data not shown). Although poliovirus RdRp forms a dimer (15), the interface is different from that observed for BVDV polymerase. Although these results indicate that the crystallographic dimer is not biologically relevant, the buried surface area created by dimerization is 2,815 Å^2, suggesting a moderately strong interaction. Thus, it is possible that the dimer might play a significant role when it is a part of the replicase complex.

A second BVDV inhibitor, compound 1453, inhibits replication in the membrane-bound replicase complex but does not inhibit polymerase activity *in vitro* (39). However, a drug-resistant variant has a Gly substituted for the Glu at position 291, suggesting that Glu-291 may be involved in protein–protein interactions in the replicase complex. Glu-291, which is 7 Å away from Phe-224, is located in a short loop in the fingers domain, close to the fingertip region. The observation that both Phe-224 and Glu-291 are located on the same surface of the fingers domain, coupled with the higher potency of the compounds in replicase complex assays compared to purified polymerase assays, suggests that the top of the fingers domain may be a protein-binding site important for interaction with other proteins, such as the NS3 helicase, in the replicase complex (24, 41, 42). Hence, the antiviral compounds might interfere with the assembly of this complex.

The BVDV Polymerase Mechanism. RNA synthesis by RdRp involves template binding, initiation complex formation, and transition from initiation to elongation. The selectivity of RdRps for template binding and initiating RNA synthesis *de novo* or using a primer may be controlled by the thumb domain. BVDV, HCV, and ϕ6 polymerases, which all use ssRNA templates and initiate *de novo*, have an elaborate thumb domain architecture, with loops protruding into the active site. In contrast, poliovirus and calicivirus polymerases, which use a protein-linked primer and template, have a smaller thumb domain and, thus, a larger template-binding channel.

Upon binding of the template and GTP, a *de novo* initiation complex is formed. NTPs complementary to the 3′ end of the template base form Watson–Crick base pairs. The triphosphate of the incoming NTP is held in place by two metal ions, which are also coordinated by the aspartic residue in the conserved GDD motif (RdRp motif VI). The NTP at the *i* (priming) site is selected by base pairing with the 3′ end terminal base of the template. A special GTP, required for initiation, mimics a nascent strand at the $i-1$ site, thereby positioning the 3′-OH of its sugar moiety close to the ribose of the NTP at the *i* site. This NTP will become the first nucleotide of the new complementary RNA strand. The correctly oriented 3′-OH group of the *i* site NTP then attacks the α-phosphate of the incoming NTP at the $i + 1$ (catalytic) site to form a new phosphodiester bond.

The translocation of the template RNA and product RNA may be facilitated by the flexible fingertip region, which contributes to the binding of an NTP at the $i + 1$ site, in combination with the C-terminal loop of the thumb domain. Subsequently, NTPs are added to the newly synthesized product RNA strand as the nucleotidyl transfer process is repeated until the template RNA is completely copied.

We thank the Advanced Photon Source 14ID and Cornell High Energy Synchrotron Source F1 beamline staff for assistance with data collection. We thank Drs. Marc Morais and Shuji Kanamaru for helpful discussions and Cheryl Towell and Sharon Wilder for help in the preparation of the manuscript. This work benefited from a Purdue University reinvestment fund award and Program Project Grant AI 55672 (to R.J.K., J.L.S., and M.G.R.). K.H.C. was supported by the Purdue University Trask Fund.

1. Paul, A. V., Van Boom, J. H., Filippov, D. & Wimmer, E. (1998) *Nature* **393,** 280–284.
2. Kao, C. C., Singh, P. & Eckert, D. J. (2001) *Virology* **287,** 251–260.
3. Kao, C. C., Del Vecchio, A. M. & Zhong, W. (1999) *Virology* **253,** 1–7.
4. Luo, G., Hamatake, R. K., Mathis, D. M., Racela, J., Rigat, K., Lemm, J. & Colonno, R. J. (2000) *J. Virol.* **74,** 851–863.
5. Nomaguchi, M., Ackerman, M., Yon, C., You, S. & Padmanbhan, R. (2003) *J. Virol.* **77,** 8831–8842.
6. Yi, G.-H., Zhang, C.-Y., Cao, S., Wu, H.-X. & Wang, Y. (2003) *Eur. J. Biochem.* **270,** 4952–4961.
7. Lindenbach, B. D. & Rice, C. M. (2001) in *Fields Virology*, eds. Knipe, D. M. & Howley, P. M. (Lippincott Williams & Wilkins, Philadelphia), pp. 991–1041.
8. Meyers, G. & Thiel, H. J. (1996) *Adv. Virus Res.* **47,** 53–118.
9. Ago, H., Adachi, T., Yoshida, A., Yamamoto, M., Habuka, N., Yatsunami, K. & Miyano, M. (1999) *Structure (Cambridge, U.K.)* **7,** 1417–1426.
10. Lesburg, C. A., Cable, M. B., Ferrari, E., Hong, Z., Mannarino, A. & Weber, P. C. (1999) *Nat. Struct. Biol.* **6,** 937–942.
11. Bressanelli, S., Tomei, L., Roussel, A., Incitti, I., Vitale, R. L., Mathieu, M., De Francesco, R. & Rey, F. A. (1999) *Proc. Natl. Acad. Sci. USA* **96,** 13034–13039.
12. Bressanelli, S., Tomei, L., Rey, F. A. & De Francesco, R. (2002) *J. Virol.* **76,** 3482–3492.
13. O'Farrell, D., Trowbridge, R., Rowlands, D. & Jäger, J. (2003) *J. Mol. Biol.* **326,** 1025–1035.
14. Ng, K. K. S., Cherney, M. M., Vázquez, A. L., Machín, A., Alonso, J. M. M., Parra, F. & James, M. N. G. (2002) *J. Biol. Chem.* **277,** 1381–1387.
15. Hansen, J. L., Long, A. M. & Schultz, S. C. (1997) *Structure (Cambridge, U.K.)* **5,** 1109–1122.
16. Butcher, S. J., Grimes, J. M., Makeyev, E. V., Bamford, D. H. & Stuart, D. I. (2001) *Nature* **410,** 235–240.
17. Tao, Y., Farsetta, D. L., Nibert, M. L. & Harrison, S. C. (2002) *Cell* **111,** 733–745.
18. Ollis, D. L., Brick, P., Hamlin, R., Xuong, N. G. & Steitz, T. A. (1985) *Nature* **313,** 762–766.
19. Kohlstaedt, L. A., Wang, J., Friedman, J. M., Rice, P. A. & Steitz, T. A. (1992) *Science* **256,** 1783–1790.
20. Huang, H., Chopra, R., Verdine, G. L. & Harrison, S. C. (1998) *Science* **282,** 1669–1675.
21. Ren, J., Esnouf, R., Hopkins, A., Ross, C., Jones, Y., Stammers, D. & Stuart, D. (1995) *Structure (Cambridge, U.K.)* **3,** 915–926.
22. Jacobo-Molina, A., Ding, J., Nanni, R. G., Clark, A. D., Jr., Lu, X., Tantillo, C., Williams, R. L., Kamer, G., Ferris, A. L., Clark, P., *et al.* (1993) *Proc. Natl. Acad. Sci. USA* **90,** 6320–6324.
23. Koonin, E. V. (1991) *J. Gen. Virol.* **72,** 2197–2206.
24. Kapoor, M., Zhang, L., Ramachandra, M., Kusukawa, J., Ebner, K. E. & Padmanabhan, R. (1995) *J. Biol. Chem.* **270,** 19100–19106.
25. Ausubel, F., Brent, R., Kingston, R. E., Moore, D. D., Seidman, J. G., Smith, J. A. & Struhl, K. (1997) *Short Protocols in Molecular Biology* (Wiley, New York).
26. Otwinowski, Z. & Minor, W. (1997) *Methods Enzymol.* **276,** 307–326.
27. Terwilliger, T. C. & Berendzen, J. (1999) *Acta Crystallogr. D* **55,** 849–861.
28. Jones, T. A., Zou, J. Y., Cowan, S. W. & Kjeldgaard, M. (1991) *Acta Crystallogr. A* **47,** 110–119.
29. Brünger, A. T., Adams, P. D., Clore, G. M., DeLano, W. L., Gros, P., Grosse-Kunstleve, R. W., Jiang, J. S., Kuszewski, J., Nilges, M., Pannu, N. S., *et al.* (1998) *Acta Crystallogr. D* **54,** 905–921.
30. Rossmann, M. G. (1990) *Acta Crystallogr. A* **46,** 73–82.
31. Navaza, J. (1994) *Acta Crystallogr. A* **50,** 157–163.
32. Poch, O., Sauvaget, I., Delarue, M. & Tordo, N. (1989) *EMBO J.* **8,** 3867–3874.
33. Lai, V. C. H., Kao, C. C., Ferrari, E., Park, J., Uss, A. S., Wright-Minogue, J., Hong, Z. & Lau, J. Y. N. (1999) *J. Virol.* **73,** 10129–10136.
34. Hong, Z., Cameron, C. E., Walker, M. P., Castro, C., Yao, N., Lau, J. Y. N. & Zhong, W. (2001) *Virology* **285,** 6–11.
35. Shirako, Y., Strauss, E. G. & Strauss, J. H. (2000) *Virology* **276,** 148–160.
36. Ranjith-Kumar, C. T., Gutshall, L., Kim, M.-J., Sarisky, R. T. & Kao, C. C. (2002) *J. Virol.* **76,** 12526–12536.
37. Ranjith-Kumar, C. T., Gutshall, L., Sarisky, R. T. & Kao, C. C. (2003) *J. Mol. Biol.* **330,** 675–685.
38. Baginski, S. C., Pevear, D. C., Seipel, M., Sun, S. C. C., Benetatos, C. A., Chunduru, S. K., Rice, C. M. & Collett, M. S. (2000) *Proc. Natl. Acad. Sci. USA* **97,** 7981–7986.
39. Sun, J.-H., Lemm, J. A., O'Boyle, D. R., II, Racela, J., Colonno, R. J. & Gao, M. (2003) *J. Virol.* **77,** 6753–6760.
40. Lewis, J. K., Bothner, B., Smith, T. J. & Siuzdak, G. (1998) *Proc. Natl. Acad. Sci. USA* **95,** 6774–6778.
41. Piccininni, S., Varaklioti, A., Nardell, M., Dave, B., Raney, K. D. & McCarthy, J. E. G. (2002) *J. Biol. Chem.* **277,** 45670–45679.
42. Dimitrova, M., Imbert, I., Kieny, M. P. & Schuster, C. (2003) *J. Virol.* **77,** 5401–5414.